Journal of Drug Delivery Science and Technology 58 (2020) 101562

Contents lists available at ScienceDirect

Journal of Drug Delivery Science and Technology

journal homepage: www.elsevier.com/locate/jddst

Formation of Diacerein − fumaric acid eutectic as a multi-component system for the functionality enhancement

Rajeshri D. Patel[a], Mihir K. Raval[a,*], Navin R. Sheth[b]

[a] Department of Pharmaceutical Sciences, Saurashtra University, Rajkot, 360 005, Gujarat, India
[b] Gujarat Technological University, Ahmedabad, 382 424, Gujarat, India

ARTICLE INFO

Keywords:
Diacerein
Fumaric acid
Crystal engineering
Tabletability
Phase diagram
Tammann's triangle
Physico-mechanical properties

ABSTRACT

The present study aimed to enhance physico-mechanical properties of poorly soluble drug Diacerein (DIA) using crystal engineering approach. Fumaric acid (FMA) was competent enough to generate a novel solid form of DIA by acetone assisted grinding method and was fully characterized. A lower melting depression and maximum enthalpy of fusion resulted from phase diagram and Tammann's triangle of binary system revealed the formation of eutectic mixture with molar ratio of 1: 2 (DIA: FMA). It was further confirmed by PXRD and FT-IR spectra. The topographical differences were observed in case of eutectic by SEM analysis imparting its better flow and packability. Pharmaceutical behaviors in terms of solubility, dissolution, tabletability, compressibility and stability suggested superior functionality of eutectic compared to DIA alone. Pharmacokinetic study of eutectic demonstrated 1.77 times greater bioavailability. Thus, the concept of crystal engineering was successful to prepare DIA-FMA eutectic as a potential way for improving material functionality.

1. Introduction

Biopharmaceutical classification system (BCS) has become an important system to categorize active pharmaceutical ingredients (APIs) based on their aqueous solubility and membrane permeability. Major portion of the candidates from the drug development pipeline exhibit the bioavailability constraint and fall under class II (70%) and class IV (20%) categories. In context to this, drug candidates despite having desired pharmacological activity face various difficulties in the development and commercialization phase due to their unfavorable solubility, bioavailability, stability toward thermal and humidity stress, flowability, manufacturability and pharmacokinetics parameters and so on [1]. Development of a successful solid dosage form is the result of the comprehensive knowledge about the aforementioned pharmaceutical properties of APIs and making use of this knowledge to formulate a tailor-made technique to optimize these parameters for an individual API [2,3].

Now a days, crystal engineering has served as the trailblazer approach in the development of stubborn APIs with poor pharmaceutical relevant properties into a classic product without changing the efficacy [4]. The detection of the best solid state form adopting the principle of crystal engineering approach has extensively been employed in supramolecular chemistry [5]. It mainly associates the formation of novel salt, polymorphs, solvate, hydrate, cocrystal, eutectic, solid solution, amorphous, and co-amorphous system. Perhaps, salt formation can modify the pharmaceutical properties of ionisable APIs through covalent bonding while remaining multi-component solid forms can effectively improve the aforesaid properties of non-ionisable or poorly ionisable APIs with counter molecule/coformer using non-covalent interaction such as hydrogen bonding, π-π stacking, dipole interaction or van der waals forces [6].

In line to this discussion, a eutectic mixture, conglomerate of solid solutions, is a multi-component crystalline adduct which undergoes melting at a lower temperature than that of the individual components. Though, eutectic systems have been shown to yield better pharmaceutical behaviour of APIs, a very few studies incorporated use of a eutectic system [7]. In our previous study, we have investigated the formation of eutectic to improve the functionality of nimesulide with nicotinamide as a coformer [8]. Further, literature search revealed some interesting studies on improvement in diverse pharmaceutical properties of APIs using eutectic system as the core approach such as enhancement in biological efficacy of hesperetin by preparing highly soluble eutectics [9], improvement in physicochemical and pharmacokinetic behavior of α-eprosartan by formation of eutectic [10], better

Abbreviations: DIA, Diacerein; FMA, Fumaric acid; DSC, differential scanning calorimetry; PXRD, powder X-ray diffraction; FT-IR, Fourier transform infrared spectroscopy; SEM, scanning electron microscopy

* Corresponding author.
E-mail addresses: rajeshripatel.2504@gmail.com (R.D. Patel), mkraval@sauuni.ac.in (M.K. Raval), navin_sheth@yahoo.com (N.R. Sheth).

https://doi.org/10.1016/j.jddst.2020.101562
Received 16 December 2019; Received in revised form 26 January 2020; Accepted 30 January 2020
Available online 04 February 2020
1773-2247/

solubility profile of curcumin was achieved through eutectic formation approach [11], Bansal and his team showed that the microstructure of aspirin-paracetamol eutectic system presented superior compressibility, tabletability, and compactibility of the system [12]. Various other drug-drug eutectics such as simvastatin-aspirin [13], etodolac with paracetamol and propranolol hydrochloride [14], hydrochlorothiazide-atenolol [15], and felodipine-nicotinamide [9] have also been studied for their improved pharmaceutical properties.

Diacerein (DIA) and its active metabolite rhein are anthraquinone derivatives that have been used for the treatment of osteoarthritis [16]. DIA entirely converts into rhein before reaching the systemic circulation [17]. DIA is a crystalline yellow powder with a melting point 255.2 °C, molecular weight of 368.3 g/mol, and LogP of 2.4. DIA shows poor solubility (3.197 mg/L) and belongs to BCS class II which creates the problem in the oral bioavailability (35–56%) [18]. Moreover, DIA exhibits poor mechanical characteristic with respect to flow and compressibility [19]. Various formulation approaches such as nano-suspension [20], solid dispersion [21], complexation [19], nanoparticles [22], and nanofiber [23] were reported to improve the pharmaceutical performance of DIA, and however, to the best of our knowledge there are no studies available on eutectic form of DIA.

In the light of above background, the present study was designed to prepare a novel eutectic of DIA with fumaric acid (FMA) as a coformer. FMA is listed as a Generally Recognized as Safe (GRAS) coformer and the presence of the aliphatic carboxylic acid group makes it a good melting point modulator [24]. The study was extended to explore the effect of prepared eutectic on the biopharmaceutical performance of DIA alone and in the tablet dosage form.

2. Materials and methods

2.1. Materials

DIA (API) was generously provided by Ami Lifesciences Pvt. Ltd. (Baroda, India) with batch no. DSN/40400615. FMA (Coformer) was purchased from Sisco Research Laboratories Pvt. Ltd. (Mumbai, India). Fig. 1 depicts chemical structures of DIA and FMA. Rhein (Active metabolite of DIA) was procured from Yucca Enterprises (Wadala, Mumbai). Acetone and acetonitrile (HPLC grade) were obtained from Merck Pvt. LTD. (Mumbai, India). All other chemicals and solvents used were of chromatographical or analytical grade. Water was purified using Milli-Q water purification system (Merck Millipore Pvt. Ltd., India).

2.2. Preparation and determination of eutectic point

Binary mixtures of DIA/FMA in various mole fractions ranging from 0 to 1 (corresponding to the molar ratios of 1:3, 1:2, 1:1, 2:1 and 3:1) were manually grounded for 20 min in an agate mortar pestle (nearly 200 mg batch scale) with periodically addition of few drops of acetone (≈200 μL). The resulted dried mass was sieved through a 100 mesh sieve (ASTM standard) and placed in the desiccator containing silica gel. The obtained materials were subjected to thermal analysis by Differential Scanning Calorimetry (DSC) for ascertaining the formation of multi-component solid forms. The obtained solidus and liquidus melting points from DSC curves were used to construct the phase diagram for elucidating the molar ratio of the binary system [25]. As the molar ratio for the binary composition was still unclear, Tammann's triangle was generated by plotting values of eutectic melting enthalpy against the various mole fractions of drug to confirm the optimum eutectic composition [26,27].

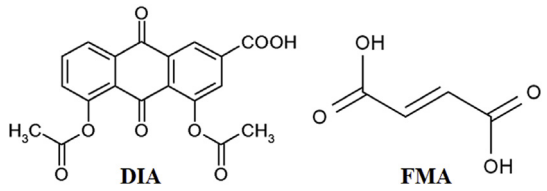

Fig. 1. Chemical structures of Diacerein (DIA) and Fumaric acid (FMA).

2.3. Solid state characterization

2.3.1. Thermal analysis

Thermal analysis was performed with help of DSC (DSC 60, Shimadzu, Japan). A precise amount of weighed samples (2–3 mg) were sealed in aluminium pans using an empty pan as a reference and analyzed from 40 to 300 °C at a scan speed of 5 °C/min under inert conditions maintained by purging nitrogen gas at a flow rate of 100 mL/min. The recorded data was collected and analyzed using Shimadzu TA 60 software.

2.3.2. X-ray powder diffraction (PXRD)

The PXRD study was performed on an X'Pert PRO Multi-Purpose Diffractometer (PANalytical Diffractometer, Netherlands) with Cu-Kα X-radiation at voltage 40 kV and current 30 mA. X'Pert HighScore Plus software was used to collect and plot the diffraction patterns. The instrument was operated over 2θ range of 10–40° at a scan rate of 0.0499°/s.

2.3.3. Fourier transform infrared (FTIR) spectroscopy

FT-IR spectroscopy (Cary-630, Agilent Technologies, USA) was employed for collecting the IR spectra of the grounded samples. The spectra were recorded using the ATR technique (Diamond ATR crystal, Agilent Technologies, USA) and collected by the Lab solution software. The IR spectrum was acquired over the range of 400–4000 cm^{-1} with 4 accumulative scans having resolution of 4 cm^{-1}.

2.3.4. Scanning electron microscopy (SEM)

The SEM images of pure components and the prepared samples were taken on a SEM (JSM-6380, Jeol, Japan) operating at 10 kV with image analyzer. Briefly, the samples were dispersed on an aluminum stub with double-faced adhesive tape. The mounted samples were made electrically conductive by coating the powder with a thin layer of gold using sputter coater instrument. Thus prepared stubs were placed in the microscope and the images were observed and recorded at the magnification range of 1,000 X to 10,000 X.

2.4. Powder characterization

2.4.1. Kawakita and Kuno's analysis

Kawakita and Kuno's analysis address the powder packability and degree of volume reduction. Prior to analysis, all the samples were sieved through 100-mesh sieve to reduce the possible effect of particle size. Briefly, bulk and tapped densities of powder samples were calculated from the change in volume of powder level into a 100 mL measuring cylinder, recorded after 100, 300, 500, 750, 1200 to 2000 taps in a tap density tester USP (Electrolab, ETD-1020, India). The packability was estimated using modified Kawakita equation as follows (Eq. (1)).

$$\frac{n}{c} = \frac{n}{a} + \frac{1}{ab} \quad (1)$$

where, n = tap number; c = volume reduction; c can be calculated according to Eq. (2).

$$c = \frac{V_0 - V_n}{V_0} \quad (2)$$

where, V_0 and V_n are the powder bed volumes at initial and nth tapped state, respectively. a and b are the Kawakita constants; *'a'* defines as initial porosity of the powder which explains total degree of volume reduction for the bed of particles at infinite applied pressure and *'1/b'*

expresses pressure needed to compress the powder to one half of the total volume. The values of *'a'* and *'b'* were calculated from the slope and intercept of the Kawakita plot of $\frac{n}{c}$ Vs *n*, respectively [28]. The data produced in Kawakita equation was analyzed by Kuno's equation (Eq. (3)):

$$\ln(qt - qn) = - Kn + \ln (qt - q0) \quad (3)$$

where, *q0*, *qn*, and *qt* are the initial density, density at 'nth' taps and density at infinite taps, respectively. *Kn* is the Kuno's constant represents rate of packing process. The packability of powder expresses by evaluating *a, 1/b*, and *Kn*. Additionally, Rearrangement index (ab index) accesses the evaluation of particle rearrangement during compression which is derived from the Kawakita constants *'a'* and *'b'*. The ab index was calculated as the reciprocal of the intercept of the extrapolated part of the Kawakita plots [29].

2.4.2. Heckel plot

The Heckel plot illustrates the force and displacement data to a linear relationship for the powders undergoing compaction. The compacts were prepared by adding a small amount of 2% w/w microcrystalline cellulose-102 (MCC) as binder to the pure drug and eutectic sample with accurately weighing 200 ± 5 mg for each sample. The prepared powders manually filled into 10-mm flat-faced punch in KBr press (Techno-search Instruments, India) and compressed under various compression force ranging from 1 to 9 tons (9.8×10^3 to 88.26×10^3 N) by keeping 1 min dwell time. The punch and die were lubricated using 1% w/v suspension of magnesium stearate in acetone prior a compaction process [30]. True density was considered as mass per volume of the compact at a maximum applied force in tons (Here, 9 tons) [31].

$$ln\left[\frac{1}{(1-D)}\right] = KP + A \quad (4)$$

Here, D ($= \rho_A/\rho_T$) is the relative density of compacts at applied pressure *P*; ρ_A and ρ_T are the density at pressure P and true density, respectively; 1-D indicates the porosity (ε) of powder; K (slope) and A (Y-intercept) are the Heckel constants obtained by plotting the graph of *ln [1/(1-D)]* Vs *P* curve i.e. Heckel plot. Reciprocal of *K* denotes mean yield pressure (Py) and *A* expresses the densification of powder bed at low pressure. Yield strength (σ0) represents the material ability to undergo deformation or fragmentation. It can be calculated by 1/3 *K*.

2.4.3. Powder tabletability

Powder tabletability was evaluated by plotting tensile strength (T, Kg) of the compacts as a function of compaction pressure [32]. The prepared compacts in the Heckel analysis were subjected for the tensile strength measurement as follows (Eq. (5)).

$$T = \frac{0.0624 \times P}{D \times T} \quad (5)$$

where, diameter (*D*) and thickness (*T*) were measured using a digital vernier caliper (Mitutoyo, Japan) after 24 h of compaction, and a crushing strength (*P*) was measured with the help of digital hardness tester (Electrolab Pvt. Ltd., India). The elastic recovery was performed for determining the retained energy during the compression process and released after compression process. The elastic recovery can be calculated using the thickness before (*Hc*) and after (*He*) being stored for 24 h using Eq. (6) [33].

$$\%\, ER = \left[\frac{H_e - H_c}{H_c}\right] \times 100 \quad \%ER = \left[\frac{(H_e - H_c)}{H_c}\right] \times 100 \quad (6)$$

Table 1
Manufacturing formulas for the preparation of directly compressible tablets.

Ingredients	Amount per tablet (mg)	
	DIA	DIA-FMA Eutectic
Diacerein IP	50	81.6 (equivalent to 50 mg DIA)
Lactose monohydrate	115	103.4
Microcrystalline cellulose-102 (MCC)	25	5
Aerosil-200	25	25
Sodium starch glycolate	25	25
Magnesium stearate	5	5
Talc	5	5
Total weight of tablet	**250**	**250**

2.5. Formulation and evaluation of directly compressible tablets

Tablets of raw DIA and DIA-FMA samples were formulated using direct compression method and manufacturing formulae of the prepared tablets are given in Table 1. The specific amounts of sieved pure DIA and prepared sample were mixed separately with sufficient portions of pharmaceutical excipients to prepare approximately 40 tablets from each batch. The individual blends were introduced manually into the die and compressed by 12 mm round and concave faced punch using eight-station rotary tablet machine (Karnawati Engineering Ltd., India). The tablets were ejected and stored in screw-capped bottles for 24 h, to allow for possible hardening and elastic recovery. The tablets were also sampled for in-process and finished product evaluation tests. Weight variation test was carried out by weighing 20 tablets individually and then calculating the average weight. Thickness of the tablets was obtained by Mitutoyo caliper. Hardness and friability of tablets were measured with the help of digital hardness tester and Roche friabilator (EF-2, Electrolab Pvt. Ltd., India), respectively. Disintegration test was performed for six tablets using disintegration test apparatus (ED2, Electrolab Pvt. Ltd., India) at 37 ± 1 °C in 900 mL of distilled water in accordance with the Indian Pharmacopoeia 2010 [34].

2.6. High performance liquid chromatography (HPLC) method development

Drug and conformer were quantified using HPLC system (Shimadzu Corporation, Japan) which consisted of a LC-20AD solvent delivery system, a DGU-20A5R vacuum degasser, a CTO-20AC thermostated column oven and SIL20AC autosampler, and coupled with a SPD-M 20A PDA detector. The Lab solution software (version 5.53 SP3C) was used for the analysis of the data. Phenomenex Gemini C18 column (250 mm × 4.6 mm, 5 μ) placed in thermostated column oven at 40 °C was used for chromatographic separation. The mobile phase, comprising of acetonitrile (ACN; A) and ammonium acetate buffer (10 mM; pH 3; B), was eluted through the gradient system as follows: 80%→30% B at 0.0–8.0 min; 30%→60% B at 8.0–12.0 min; 60%→80% B at 12.0–14.0 min. The details of the developed HPLC method are described in Table S1, see in supplementary data.

2.7. Drug content determination

Drug content of DIA in the prepared eutectic was estimated by dissolving 10 mg of the prepared samples in 1 mL of DMSO and further diluted up to 10 mL with ACN. After appropriate dilution, the samples were analyzed using HPLC method as mentioned above. Content determination of drug in each sample was performed in triplicate and the average and standard deviation were calculated.

2.8. Solubility measurement of various molar compositions

Solubility of DIA and different molar ratios (1:1, 1:2, 1:3, 2:1, 3:1) of

DIA-FMA samples was measured in distilled water using shake flask method. Approximately 50 mg of DIA (corresponding to, for DIA-FMA samples) were placed in a flask containing 200 mL distilled water. The resultant dispersions were kept in a shaker-incubator equipped with a temperature controlling system (Tempo Instruments and Equipments Pvt. Ltd., India) at 37 ± 0.5 °C with a speed of 150 rpm for 24 h to allow saturation. Sample aliquots (5 mL) were taken from the dispersion at the predefined time intervals (5, 10, 15, 30, 45, and 60 min), and replaced by equal volume of distilled water. The resulting samples were filtered through 0.45 μm syringe filter (Millex-HV, Millipore) and the filtrate was suitably diluted and analyzed by HPLC method for the quantification of drug in all samples as per section 2.6.

2.9. In-vitro drug release profile

In-vitro drug release profiles of pure DIA and DIA-FMA prepared samples (USP type-I apparatus) and their formulations (USP type-II apparatus) were performed using USP dissolution test apparatus (USP Electrolab TDT-06P, India). The dissolution profiles of all the samples were evaluated in dissolution vessels containing 900 mL of citrate buffer (pH 6) at 75 rpm maintained at 37 ± 0.5 °C [34]. Aliquots (5 mL) were withdrawn from the vessels at the scheduled intervals and the dissolution media was replenished with equal volume of fresh media to maintain sink condition. The samples were filtered immediately through 0.45 μm syringe filter and drug concentration of each sample was estimated using HPLC method as described in section 2.6. The evaluation parameters of dissolution profile were achieved by plotting the cumulative amounts of drug dissolved as a function of time. The results were analyzed to ascertain dissolution percent at 5 min (% $DP_{5\ min}$) and time to release 50% of the drug ($t_{50\%}$). Overall dissolution efficiency (% DE) was measured as the area under curve (AUC) up to a certain time 't' (here, 60 min) expressed as percentage of the area of the rectangle described by 100% dissolution in the same time as presented in Eq. (7) [35].

$$\%DE = \int_0^t \frac{y.\,dt}{y_{100}t} \times 100 \quad \%\mathrm{DE} = \int_0^t \frac{\mathrm{y}.\ \mathrm{dt}}{\mathrm{y_{100}t}} \times 100 \tag{7}$$

2.9.1. Statistical analysis of the dissolution profiles

Model independent mathematical approach was employed for the statistical analysis of resulted dissolution profiles [36]. The similarity factor f_2 was measured to evaluate similarity in the percentage dissolution between two dissolution curves as expressed in Eq. (8).

$$f_2 = 50 \times \log\left[\left(1 + \left(\frac{1}{n}\right)\sum_{t=1}^{n} w_t\,(R_t - T_t)^2\right)^{-0.5} \times 100\right]$$

$$\mathrm{f_2} = 50 \times \log\left[\left(1 + \left(\frac{1}{\mathrm{n}}\right)\sum_{\mathrm{t=1}}^{\mathrm{n}} \mathrm{w_t(R_t - T_t)^2}\right)^{-0.5} \times 100\right] \tag{8}$$

where, R_t is the percentage dissolved of reference at the time point t; T is the percentage dissolved of test at the time point t; n is the number of withdrawal points. A value of 100% for the similarity factor (f_2) recommended that test and reference profiles are identical. The value between 50 and 100 indicates that the dissolution profiles are similar whereas smaller value expresses an increment in dissimilarity between release profiles.

In order to understand difference in dissolution rate of pure drug and the prepared samples, *in vitro* mean dissolution time ($MDT_{\ in\ vitro}$) was calculated (Eq. (9)). The same calculations were also applied for the prepared dosage forms.

$$MDT_{in\ vitro} = \frac{\sum_{i=1}^{n} t_{mid}\ \Delta M}{\sum_{i=1}^{n} \Delta M} \tag{9}$$

Here, i is dissolution sample number; n is number of dissolution times at time t; t_{mid} is time at the midpoint between times t_i and t_{i-1}; ΔM is amount of drug dissolved (μg) between times t_i and t_{i-1}.

2.10. Pharmacokinetic study

2.10.1. Animals

Sprague-Dawley rats (either sex) weighing 200–250 g, were housed at 24 ± 2 °C and 50–60% relative humidity (RH). The animals were kept 12 h light/dark conditions for acclimatization for one week and fasted overnight with free access to water prior the experiment. The standard food and filtered water was supplied *ad libitum*. The animal protocol was duly approved by the Institutional Animal Ethics Committee (IAEC), Saurashtra University, India (IAEC/DPS/SU/1609; dated 12th December 2016).

2.10.2. Experimental protocol

Healthy Sprague-Dawley rats were randomly distributed in two groups, each including twelve animals (n = 12). Group I and II were administered pure DIA and the prepared eutectic suspension orally in water containing 0.2% w/v sodium carboxymethyl cellulose as suspending agent at a dose equivalent to 30 mg/kg body weight of DIA, respectively. Blood samples were collected into heparinized tubes from the retro-orbital plexus of the rats at 0 (predose), 0.25, 0.5, 0.75, 1, 1.5, 2, 4, 6, 12, and 24 h after oral administration. The plasma samples were harvested by centrifugation (Centrifuge 5418R, Eppendrof AG, Germany) at 10,000 rpm for 20 min and stored at −20 °C until analysis. A simple protein precipitation method was used for the extraction of drug from the plasma samples. Briefly, 500 μL of each plasma sample was mixed with 50 mL IS, p-Aminobenzoic acid (100 μg/mL) and vortexed for 30 s. A 500 μL volume of ACN as extraction solvent was added into it and vortexed for 10 min. The resulting mixture was centrifuged at 10,000 rpm for 10 min at 4 °C. The supernatant was collected and dried it at 60 °C at oven and the dried residues were reconstituted with mobile phase (100 μL) and vortexed it for 5 min prior to the injection in HPLC system.

2.10.3. HPLC analysis for determining drug concentration in the rat plasma

Owing to the metabolic transformation from DIA into rhein, only rhein was detected in rat plasma to evaluate the pharmacokinetics after oral administration [17]. The HPLC procedures followed as described in section 2.6 with slight modification. Briefly, ACN (A) and ammonium acetate buffer (10 mM; pH 3; B) were eluted through the gradient system as follows: 80%→30% B at 0.0–8.0 min; 30%→60% B at 8.0–10.0 min; 60%→80% B at 10.0–18.0 min. The flow rate and analytical run time were set at 0.8 mL/min and 18 min respectively. Absorbance was detected at 254 nm and sample injection was 20 μL. The concentration range was as 0.2–20 μg/mL with correlation coefficient (r^2), 0.999.

2.11. Stability study

The prepared samples (powder and tablet formulation) were evaluated for accelerated stability condition for a period of six months. Samples were put in screw-capped glass bottles separately at 40 °C/75% RH in the stability chamber (SC-16 PLUS, Remi, India). At the end of the study, samples were accessed for the dissolution profiles and solid state stability by DSC, FT-IR, and PXRD analysis.

3. Results and discussion

Co-crystallization experiment is a unique supramolecular reaction to form multi-component solid forms. Understanding the development of a cocrystal or a eutectic mainly depends on several factors such as supramolecular synthons, heteromeric/homomeric interactions, functional group deposition and complementarity, interaction strength, and packing efficiency [37,38]. Here DSC technique is employed, as the

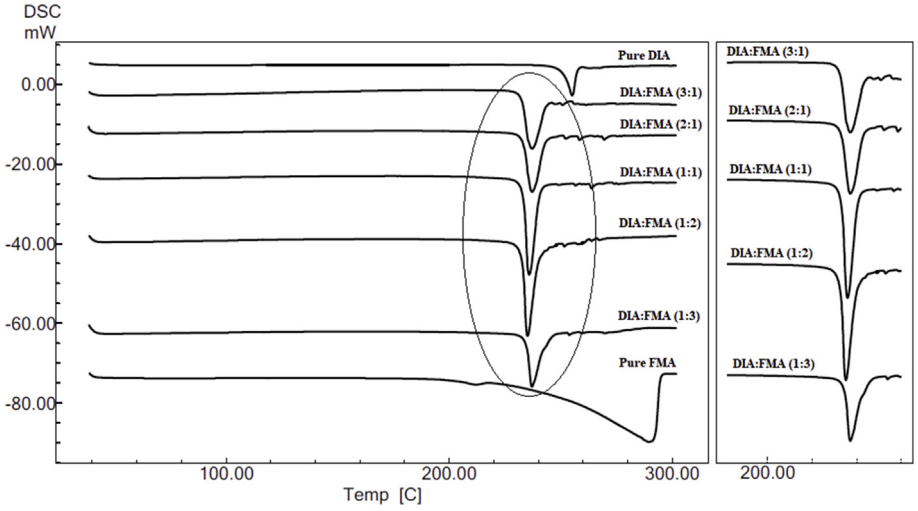

Fig. 2. Overlay of DSC enthotherms of DIA and FMA at various molar ratios.

main study method to investigate the binary phase diagram. The endothermic events from DSC curves determine the formation of multicomponent system [39]. Liquid assistant grinding experiment with its advantages of reduced time and efficient atomic reaction over neat grinding was used as a preliminary screening method to identify any interaction between drug and coformer and also to determine their stoichiometry [40]. The solvent selection was made on the basis of at least the partial solubility of drug and coformer in that particular solvent. The partial solubility of both the components was required to initiate the interaction between each other. Here, the catalytic amount of acetone was added to enhance the reaction process which readily evaporates during process itself with no leftover starting materials.

3.1. Binary phase diagram and Tammann's triangle

The DSC overlay of pure DIA, FMA, and their DIA-FMA co-ground mixtures at various mole ratios are represented in Fig. 2. The thermal properties of the pure and co-ground samples are given in Table 2. The DSC scan of DIA and FMA depicted that their melting behaviors agreed with the literature data [22,41]. It was observed that all the five ratios consistently demonstrated at the same melting behavior nearer to 233 °C, indicating as solidus temperature ($T_{Solidus}$/°C) in the binary phase diagram. Liquidus event ($T_{Liquidus}$/°C) was recognized at the higher temperature representing the complete melting of the excess participating components either drug or coformer. The binary phase diagram of DIA-FMA system with the solidus and liquidus points is shown in Fig. 3 (A). For such kind of transition, the peak position almost all mole fractions were observed very near to each other. Moreover, only single peak was shown in all the endothermic events. As can been seen, the resulting phase diagram exhibits the "V"-type pattern which is the characteristic of the eutectic formation. The mole fraction of DIA-FMA in 1:2 showed very near solidus and liquidus points along with melting point depression at 232.97 °C. To avoid any confusion, molecular interaction was further confirmed using Tammann's triangle graph as depicted in Fig. 3 (B). From Tammann's graph, it was found that the mole fraction of DIA at 0.33 which is nothing but a molar ratio of 1:2 showed maximum ΔH_{fus} value. It was confirmation of eutectic formation at 1:2 M ratio of DIA [26]. Furthermore, the ΔH_{fus} of eutectic was estimated theoretically using Eq. (10) and this was employed to determine the excess ΔH_{fus} as compared to experimental values described in Eq. (11) [42].

Table 2
Thermal properties of the pure and co-ground samples at various mole fractions of DIA.

X_{DIA}*	$T_{solidus}$/°C	$T_{liquidus}$/°C	T_{onset} (pure compounds)/°C	ΔH_{fus} (J/g)
1.00	–	–	255.17	96.68
0.75	232.71	243.38		343.26
0.67	233.02	242.67		465.57
0.50	233.47	240.41		543.57
0.33	232.97	235.16		672.93
0.25	234.74	243.00		486.76
0.00	–	–	289.48	2310.00

Temperature of solidus, $T_{solidus}$ and temperature of liquidus, $T_{liquidus}$, obtained from DSC heating runs of co-ground mixtures of DIA and FMA; mole fraction of DIA, X_{DIA}.

$$\Delta H_{fus\ (calculated)} = (X_{DIA} * \Delta H_{fus\ (DIA)}) + (X_{FMA} * \Delta H_{fus\ (FMA)}) \quad (10)$$

where.

X_{DIA} and X_{FMA} are the mole fraction of DIA and FMA, respectively and $\Delta H_{fus\ (DIA)}$ and $\Delta H_{fus\ (FMA)}$ are the enthalpy of fusion of DIA and FMA, respectively.

$$\Delta H_{fus\ (excess)} = \Delta H_{fus\ (experimental)} - \Delta H_{fus\ (calculated)} \quad (11)$$

From Eq. (10), the $\Delta H_{fus\ (calculated)}$ of eutectic was found to be 1547.70 J/g and from the DSC curves the $\Delta H_{fus\ (experimental)}$ of eutectic was observed as 672.93 J/g. Further excess enthalpy of fusion ($\Delta H_{fus\ (excess)}$) was calculated from Eq. (11) which is - 906.67 J/g. The negative value of the $\Delta H_{fus\ (excess)}$ of eutectic indicates that the prepared system was eutectic rather than physical mixture.

3.2. PXRD analysis

PXRD study is the discriminative technique to determine crystalline powder material through the unique characteristic diffraction pattern of the crystal lattice. The diffractograms did not show characteristic peaks at 2θ values more than 40°. Thus, the powder XRD patterns of DIA, FMA, DIA-FMA eutectic and physical mixture were recorded in the range of 10–40° and revealed high intensity with characteristic sharp peaks at 2θ scattered angles indicating the sign of crystalline nature as displayed in Table 3. The characteristic diffraction peaks of DIA and FMA were still noticeable in the prepared eutectic with minor and non-significant alterations in the position of the peaks (Fig. 4). It is interesting to note that all the characteristic peaks of the participating components were preserved in the diffraction pattern of eutectic with lower intensity than the physical mixture. This might be due to reduction in the crystallinity of drug [43]. PXRD patterns of the resulting samples are in harmony with the results of DSC, which excluded the

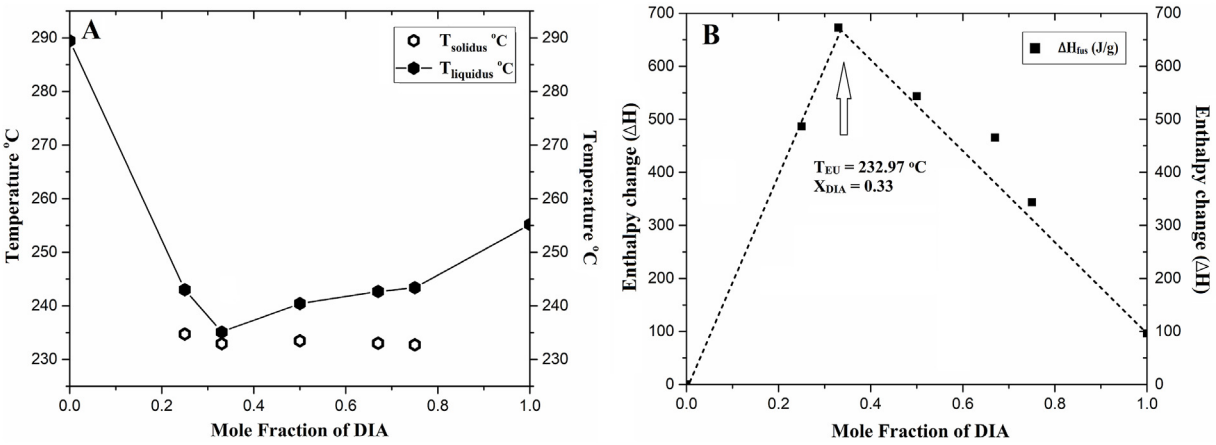

Fig. 3. Binary phase diagram (A) and Tammann's triangle graph (B) for the investigated DIA-FMA system.

Table 3
Characteristic diffraction peaks of raw materials and their prepared samples.

Sample	2 Theta (Degrees)
DIA	10.46, 17.39, 21.46, 21.90, 25.07, 27.87
FMA	22.77, 28.75, 29.38, 37.93
DIA-FMA physical mixture	10.51, 17.42, 27.93, 28.82, 37.94
DIA-FMA eutectic	22.79, 22.93, 27.93, 28.79, 29.40,

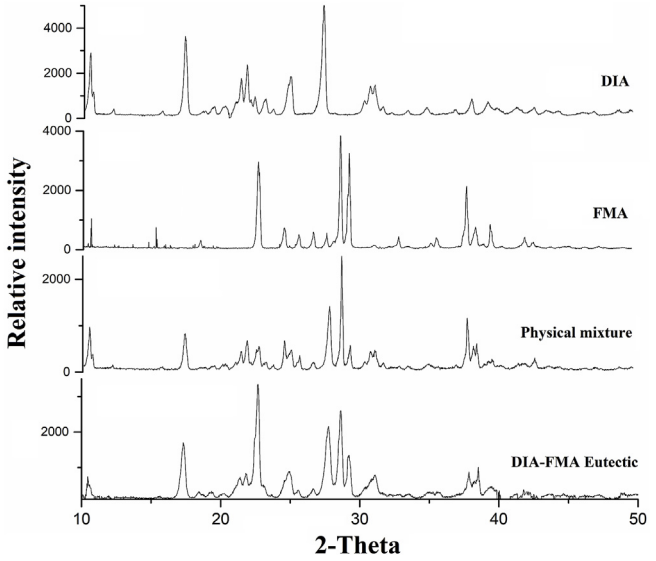

Fig. 4. Overlay of powder XRD patterns of DIA; FMA; DIA-FMA physical mixture and DIA-FMA eutectic.

existence of co-crystal and confirmed the eutectic formation [7,44].

3.3. FT-IR study

FTIR analysis is the complementary study to investigate any possible intermolecular interaction between drug and coformer in the solid state. FT-IR spectra and the assignment of major bands of pure DIA, FMA and DIA-FMA eutectic mixture are depicted in Fig. 5 and Table S2. FT-IR study of DIA-FMA eutectic expressed the summation of the characteristic vibration bands correspond to individual components without any considerable shifting reflecting the absence of significant chemical interaction. The results highlight the predominance of cohesive (homomeric; drug-drug/coformer-coformer) interaction between the components of each species in the mixture relative to adhesive (heteromeric; drug-coformer) force between the components of different species. This can also be due to shape/size misfit between the interacting molecules, thus restricting FMA molecule to establish any new supramolecular network with DIA. In addition, a 'V'-shape pattern in the binary phase diagram and no deviation in the diffraction peaks concluded the formation of eutectic rather the cocrystal [7,44].

3.4. SEM analysis

The morphological evaluation of raw DIA, FMA and DIA-FMA eutectic was done using SEM analysis as shown in Fig. 6. DIA (Fig. 6 (A)) powder was appeared acicular shaped crystalline particles with rough in surface textures which might have retarded its flowability. The SEM images of eutectic sample (C-1 & C-2) indicated platy shaped crystals with smooth surface texture compared to DIA particles. The distinct morphology of DIA-FMA eutectic with micrometer sizes represents the eutectic as a separate entity from the pure drug molecule which might be resulted in the improved processing parameters as compared to raw DIA [45].

3.5. Powder characterization

3.5.1. Kawakita and Kuno's analysis

Values of Kawakita constants *'a'* and *'1/b'* for pure drug and prepared sample are listed in Table 4 and the plot is presented in Fig. 7 (A). In this analysis, a linear relationship was monitored throughout the whole range of tapping with correlation coefficient of more than 0.99. It has been seen that the decreased value of *'a'* and increased value of *'1/b'* of prepared eutectic compared with the value of the pure DIA was an indication of the improvement in packability of the DIA-FMA sample. DIA-FMA eutectic exhibited higher values of '*Kn*' (Kuno's constant), which imparted a superior packability as compared with DIA alone [28]. Furthermore, the value of *ab* index in case of eutectic mixture was lower compared to DIA which was a sign for the requirement of less number of tapping for the particle rearrangement for the prepared eutectic [29].

3.5.2. Heckel plot study

Heckel analysis explains the densification process by plastic deformation of the powder under applied pressure following first order kinetics. Raw DIA by appearance was fluffy powder and also revealed by a lower true density when compared to prepared eutectic as shown in Table 4. Fig. 8 (dash line) illustrates the Heckel plot and its derived parameters are summarized in Table 4. Higher values of '*K*' and '*A*' of prepared eutectic over the pure DIA have better plastic behavior and increased propensity of material fragmentation which led to play significant role in void filling reflecting increased relative density in the

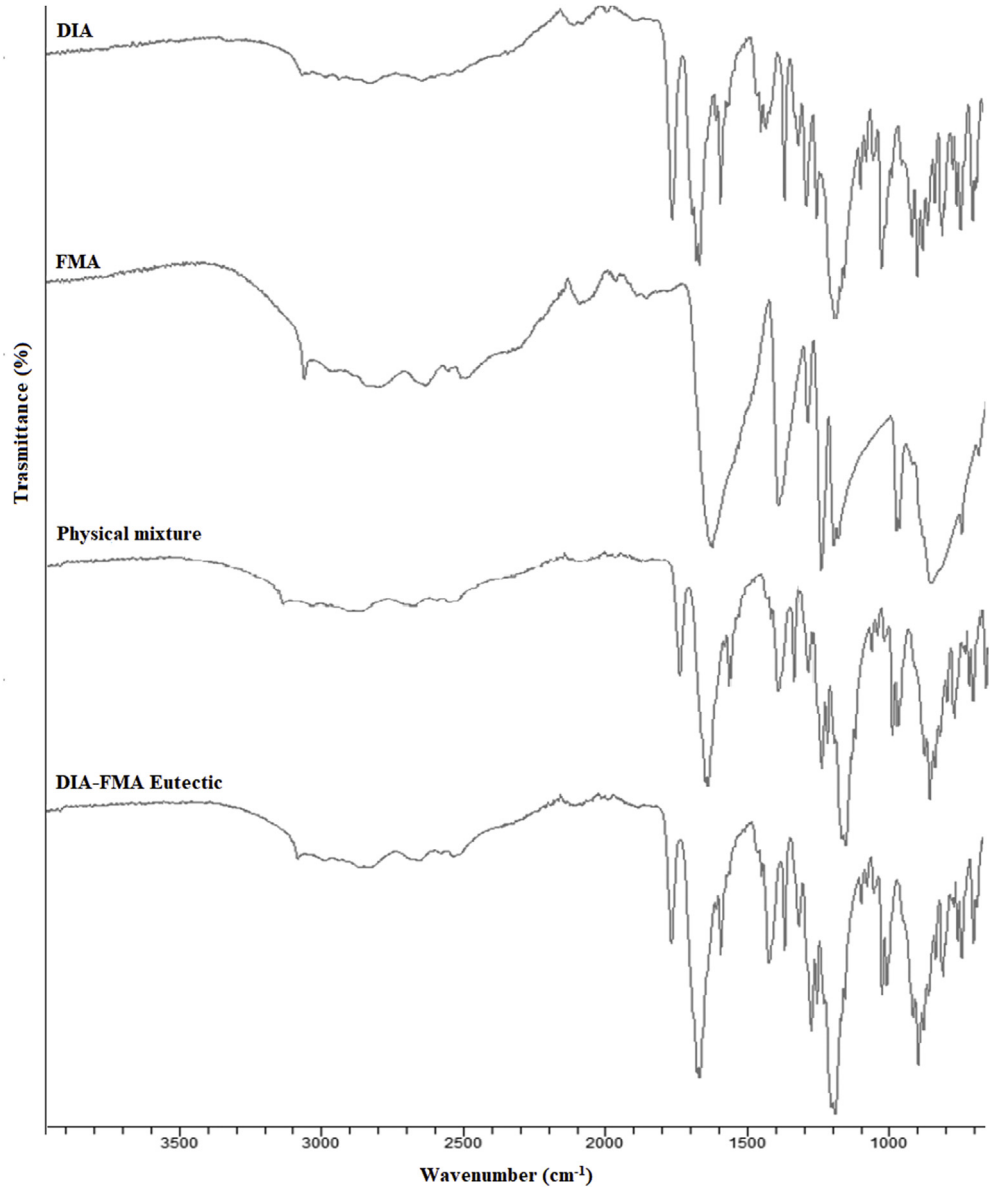

Fig. 5. FT-IR spectra of DIA; FMA; DIA-FMA physical mixture and DIA-FMA eutectic.

prepared eutectic. Another observation was made from the Heckel plot that the initial curvature in the graph was not appeared. It was a sign of a fragmentation behavior of the material. Pure DIA shows a fragmentation with very low brittleness index. Due to which a lamination was observed with even at very low compression force applied during Heckel analysis. A small amount of 2% w/w MCC as binder was added with pure drug and prepared sample followed by the Heckel study at various ascending pressures. The slope '*A*' of all the Heckel curves showed that the fragmentation and formation of new surfaces was greater in the prepared eutectic compared to DIA which resulted in greater compressibility of the eutectic sample [30]. The yield strength (σ0) and yield pressure (Py) were derived using linear regression portion of the Heckel plot ($R^2 > 0.98$ in all the samples). The lower value of Py and σ0 of eutectic sample as compared to pure drug was an indication of high degree of densification imparting good fragmentation and easy compaction property. Compressibility of the samples could be measured on the basis of porosity as a function of applied pressure as represented solid line in Fig. 8. The values of porosity attained after 9 ton force was about 9.4% and 1.5% for DIA and prepared eutectic, respectively. The above result reveals that the prepared material has become more suitable for the tablet manufacturing using direct compression technique as compared to the pure drug [46]. This outcome closely correlates with the results obtained from the '*a*' values of Kawakita plots.

3.5.3. Powder tabletability

Fig. 7 (B) depicts the higher tensile strength of prepared samples over pure drug at all compression forces. The utmost tensile strength was noticed for the compact of eutectic at 9 ton force as shown in Table 4. It indicates that eutectic material is more suitable for tabletabilty as compared to pure drug [32]. Simultaneously, % elastic recovery of DIA compacts was greater compared to prepared eutectic suggesting the lamination behavior of DIA (Table 4). By comparing elastic recovery of drug and prepared eutectic, it was clearly demonstrated that the prepared eutectic is more plastic in nature than the pure drug leading to the inter-particulate bonding which can be attributed to the presence of non-covalent intermolecular interaction [46].

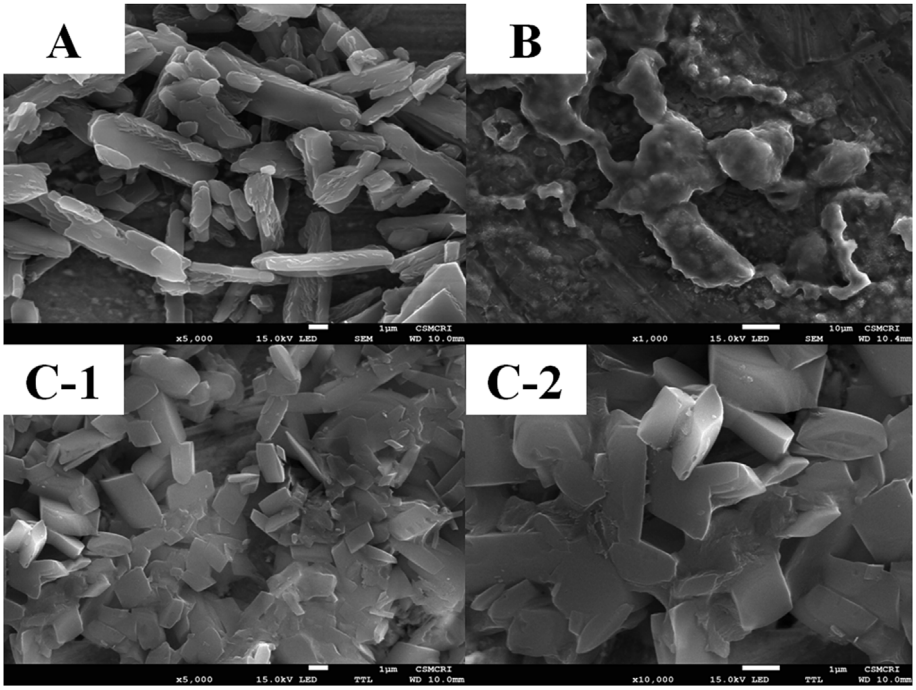

Fig. 6. SEM images of DIA (A); FMA (B) and DIA-FMA eutectic (C-1 & C-2).

Table 4
Powder characteristics of DIA and prepared eutectic.

Parameters	Pure DIA	DIA-FMA Eutectic
Kawakita plot, a (=1/slope)	0.553	0.475
1/b = intercept/slope	37.08	69.31
Kuno's constant, K	0.8696	1.0630
Rearrangement index (ab)	0.258	0.069
True density (g/cc)	1.0620	1.4195
Heckel plot constant, K	0.161	0.352
A	0.986	1.210
Yield pressure, Py	6.212	2.841
Yield strength, σ0	2.070	0.947
Tensile strength (kg/cm^2)*	6.55 ± 0.35	13.08 ± 1.27
% Elastic recovery*	2.4778 ± 1.15	1.4089 ± 0.78

*Indicates data shown as mean ± SD, (n = 3).

3.6. Post compression evaluation of directly compressible tablets

Improved powder characteristic of prepared eutectic may promote to formulate the direct compressible tablets. Here, tablets formulation of pure drug formula required 10% w/w of MCC compared to DIA-FMA eutectic formula where only 2% w/w of MCC was required. It noticeably indicated that packability, compressibility, and compactibility of the prepared eutectic were better than the pure DIA. Evaluation parameters of directly compressible tablets of pure DIA and DIA-FMA eutectic were carried out and listed in Table 5. All parameters were in good accordance with acceptance criteria [47]. The findings conclude that the physico-mechanical parameters of tablets prepared from eutectic mixture were improved compared to tablets prepared from pure DIA.

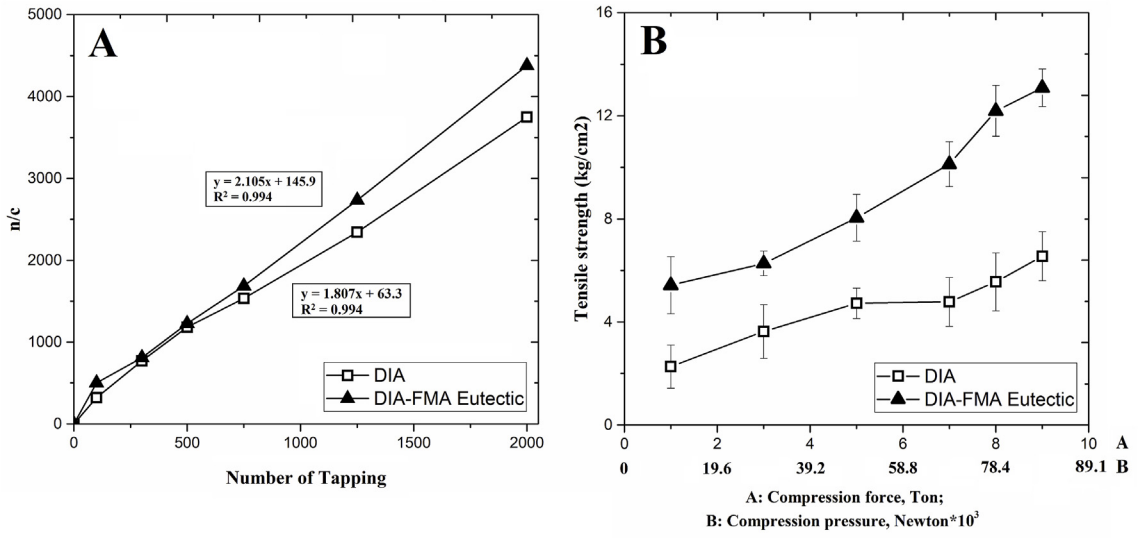

Fig. 7. Kawakita analysis (A) and powder tabletability (B) of DIA and DIA-FMA eutectic.

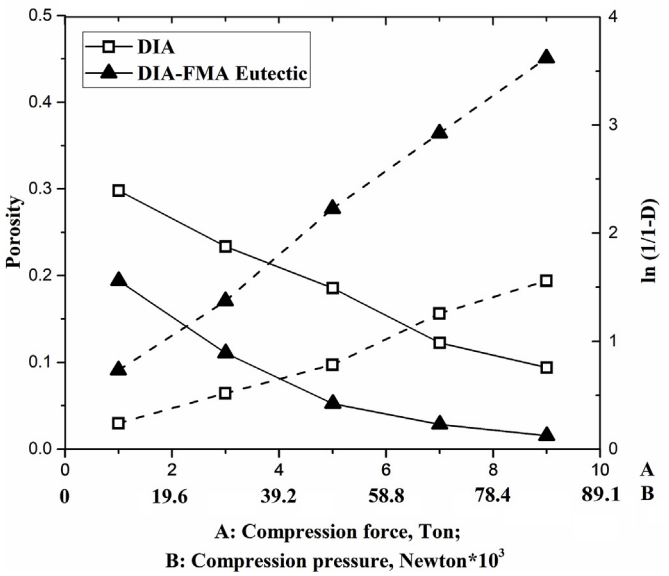

Fig. 8. Heckel plot analysis (dash line) and Compressibility study (solid line) of DIA and DIA-FMA eutectic.

Table 5
Evaluation and post dissolution parameters of directly compression tablets of pure DIA and prepared sample.

Parameters		Pure DIA	DIA-FMA Eutectic
Weight variation (mg)*		250.2 ± 2.43	249.8 ± 1.91
Thickness (mm)*		3.39 ± 0.07	3.36 ± 0.09
Hardness (kg/cm^2)*		4.9 ± 0.31	5.1 ± 0.30
Friability (% loss)*		0.36 ± 0.08	0.30 ± 0.07
D.T.(sec)*		65.33 ± 2.52	60.67 ± 4.72
% $DP_{5\ min}$	Powder	28.62	40.37$^{\#}$
	Tablet	23.42	38.83$^{\#}$
% DE	Powder	36.93	54.75$^{\#}$
	Tablet	27.50	47.54$^{\#}$
t_{50} (min)	Powder	Could not detect	15.44$^{\#}$
	Tablet		16.32$^{\#}$
f_2 Value	Powder	–	29.16
	Tablet	–	35.41
MDT, min	Powder	21.70	11.29
	Tablet	24.84	12.77

*Indicates data shown as mean ± SD, (n = 3).
$^{\#}$Implies $p < 0.05$, as compared to pure DIA.

3.7. HPLC method development

DIA shows pH dependent solubility due to the weak acidic nature, which enhances solubility at higher pH and reduces solubility at lower pH. Furthermore, it has been reported that the buffer solutions at pH ≥ 5 represented the quantification of DIA in the form of Rhein [48]. Thus, HPLC method was developed for the quantification of DIA and Rhein in presence of FMA in the prepared sample. The HPLC chromatogram demonstrated retention time (Rt) for standard solutions of DIA, FMA and Rhein to be 10.5, 4.1, and 11.6 min, respectively. (Fig. S1, see in supplementary data).

3.8. Drug content determination

Drug content of produced eutectic was found to be 87.14 ± 2.57% which showed satisfactory results. This drug content was indicated good recovery of the drug after eutectic formation.

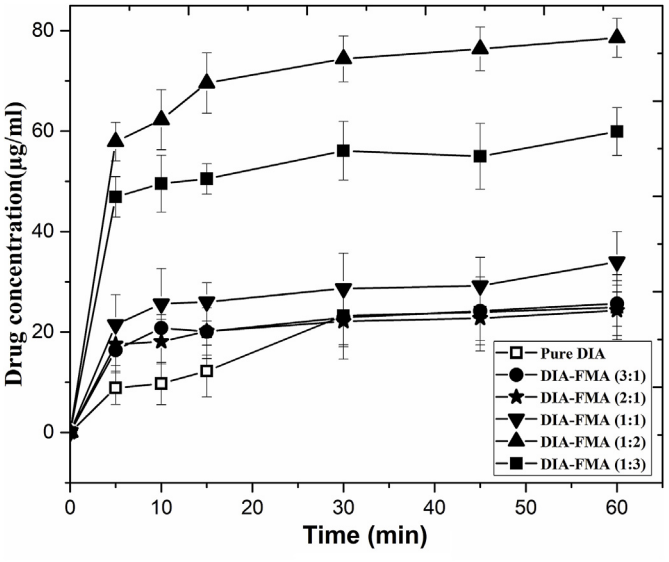

Fig. 9. Solubility measurement in various molar compositions.

3.9. Solubility measurement of various molar compositions

The solubility measurement was carried out for pure DIA and the co-ground mixtures of DIA with FMA at various ratios corresponding to 50 mg of DIA in each sample. The results of solubility profile of DIA-FMA system are illustrated in Fig. 9. As can be seen, pure DIA exhibited very slowly being dissolved within 60 min. At the same time, the solubility of the co-ground mixtures of DIA-FMA revealed significant ($P < 0.05$) improvement in all molar ratios. By comparing the kinetic solubility profiles of all the molar ratios with each other (within) and with the drug (between), it was found that molar ratio 1:2 (DIA: FMA) revealed highest kinetic behavior among the other ratios. The increment of kinetic solubility of 1:2 ratio compared to pure drug after 60 min was almost 3.15 folds. During the solubility experiment, FMA molecules diffused in the water faster than the parent DIA because the molecular weight is lesser than that of DIA as well as FMA exhibits a strong affinity towards the water molecules. Consequently, the less soluble DIA molecules become supersaturated in the solution as an amorphous phase resulting the greater solubility of prepared eutectic as compared to pure DIA [49,50].

3.10. In-vitro drug release profile

In-vitro drug release profile of powder samples exhibited that prepared eutectic showed greater drug release (71.71%) compared to raw DIA (41.70%) after 1 h (Fig. 10 (A)). The same kind of behavior was also noticed in the case of tablets prepared from pure DIA and DIA-FMA eutectic as shown in Fig. 10 (B). The quantitative analysis of dissolution profiles was estimated by calculating overall % DE, % DP_{5min} and t_{50} as expressed in Table 5. The dissolution behavior of DIA and its tablets revealed its erratic and slow drug release characteristics as reflected from the evaluation parameters of dissolution profile and hence, t_{50} could not be measured (Table 3). Such type of dissolution performance is not satisfactory for the immediate release formulation. There was a significant enhanced dissolution capacity of DIA-FMA eutectic as indicated by dissolution parameters ($P < 0.05$; Table 3). The results obtained from statistical analysis suggested that there was no similarity ($f_2 < 50$) between dissolution profiles of DIA and prepared eutectic (powder as well as tablets). Moreover, lower value of MDT for prepared eutectic compared with pure DIA demonstrated the enhancement in solubility and *in vitro* dissolution of powder and its tablet formulation. The promising enhancement in dissolution can be attributed to the presence of hydrophilic nature of coformer (FMA) which facilitates the

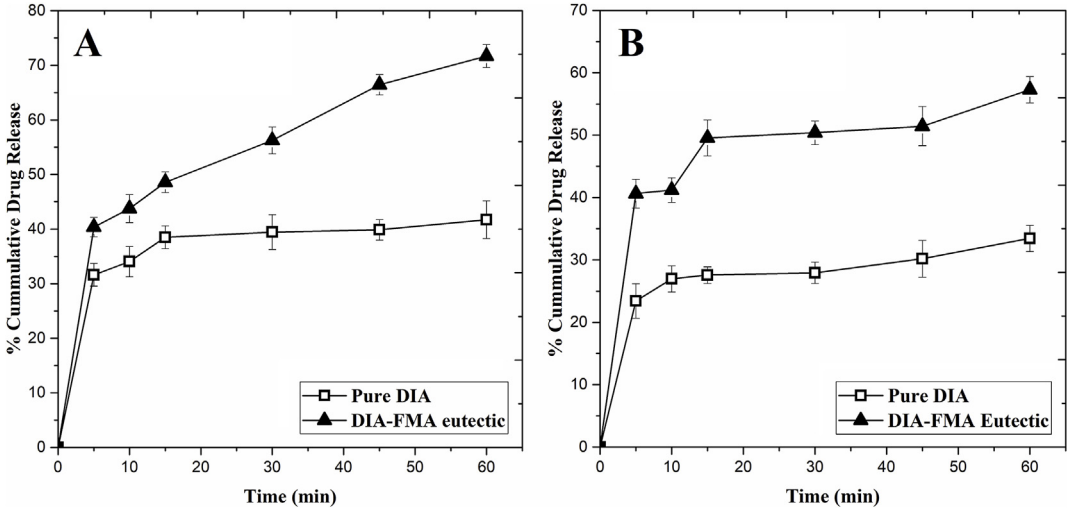

Fig. 10. *In-vitro* drug release profiles of raw DIA and DIA-FMA eutectic in powder (A) and directly compressible tablet (B).

ease of solubilisation of drug molecule in media. Moreover, melting point depression of eutectic mixture suggests the weakening of intermolecular bonds which modulates the thermodynamic functions (i.e. enthalpy, entropy, and free energy) [50,51].

3.11. Pharmacokinetic study

In accordance with the improved dissolution profiles, the eutectic system developed herein should be suitable further to screen the *in-vivo* performance of drug. Various pharmacokinetic parameters were calculated using trapezoidal rule as summarized in Table 6 and the average plasma concentration-time curves of pure drug and prepared eutectic after single oral dose administration in Sprague-Dawley rats are shown in Fig. 11. The results of pharmacokinetic evaluation suggested the superior oral bioavailability of prepared eutectic as compared to pure drug. The obtained C_{max} and $AUC_{0–24\ h}$ of prepared eutectic were increased nearly 2 and 1.5 folds, respectively and the time to reach maximum plasma concentration was diminished from 2.5 h to 2 h as compared to parent drug. Also, DIA-FMA eutectic demonstrated greater relative bioavailability (F_{rel} = $AUC_{total\text{-}eutectic}/AUC_{total\text{-}drug}$) of 1.77 indicating more oral bioavailable than the DIA [52]. The study signifies the predominance of non-covalent derivative i.e. eutectic mixture augment the biopharmaceutical behaviors of DIA.

3.12. Stability study

Physical and chemical stability study of DIA-FMA eutectic was investigated for six months under accelerated conditions (40 °C/75% RH). From the statistical analysis, the dissolution profiles of prepared eutectic (powder as well as tablet) were estimated to be similar (f_2 > 50) before and after study. Also, DSC, PXRD and IR data of eutectic showed all the characteristic peaks with no deviation in melting behavior as compared to fresh sample suggesting the stable nature of eutectic (Figs. S2, S3 and S4, see in supplementary data). Hence, the stability issue should not obstruct the commercialization of the prepared eutectic.

Table 6
Pharmacokinetic parameters of DIA and prepared eutectic after single oral dose administration to Sprague-Dawley rats.

Parameters*	DIA	DIA-FMA eutectic
C_{max} (μg/mL)	35.54 ± 5.72	70.58 ± 4.46
T_{max} (h)	2.5 ± 0.92	2 ± 0.82
$AUC_{0–24\ h}$ (μg.h/mL)	249.91 ± 152.43	453.11 ± 289.70
AUC_{total} (μg.h/mL)	298.60 ± 141.19	528.05 ± 262.63
F_{rel}	1	1.77

*Indicates data shown as mean ± SD, (n = 6).

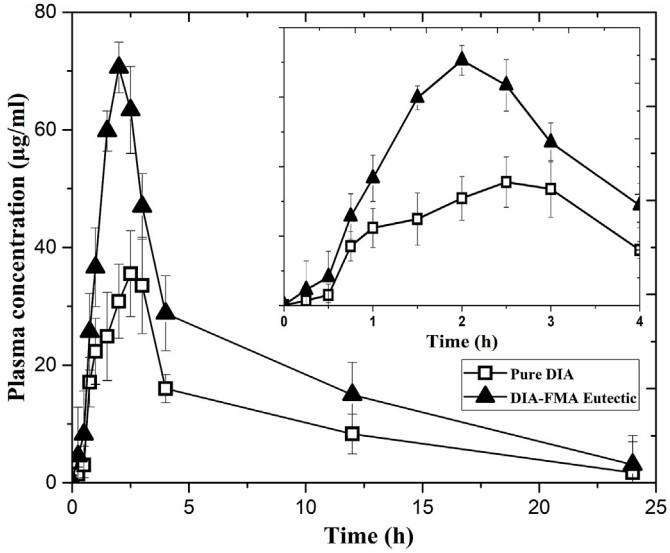

Fig. 11. Mean plasma concentration-time curves of DIA and DIA-FMA eutectic.

4. Conclusion

DIA is a BCS class II drug with poor physicochemical and pharmacokinetic parameters. In the present investigation, a eutectic system of DIA-FMA in the molar ratio of 1:2 was prepared by acetone assistant grinding technique and fully characterized. The obtained material exhibited significant enhancement in its physicochemical and powder characteristics compared to DIA alone. Additionally, this novel eutectic had superior plastic nature and good tabletability profiles than the parent drug, which was resulted in directly compressible tablets. Pharmacokinetic parameters were remarkably improved in case of the eutectic solid form along with its stable nature. The present study concluded that multi-component system can make a favorable candidate for the pharmaceutical industry with simultaneously enhanced physico-mechanical properties of poorly aqueous soluble and compressible drugs using direct compression technique.

CRediT authorship contribution statement

Rajeshri D. Patel: Investigation, Methodology, Data curation, Visualization, Formal analysis, Validation, Writing - original draft. **Mihir K. Raval:** Supervision, Conceptualization, Writing - review & editing. **Navin R. Sheth:** Writing - review & editing.

Declaration of competing interest

The authors declare that they have no conflicts of interest to disclose.

Acknowledgements

The author Ms. Rajeshri Patel gratefully acknowledges Department of Science and Technology (DST), New Delhi, India, for providing DST-INSPIRE Fellowship (IF131122) with letter no. DST/INSPIRE Fellowship/2013/1079 to carry out this research work. We are also thankful to Prof. Arvind Bansal and his Ph. D student Mr. Dnyaneshwar Kale for their continuous guidance and support throughout the study.

Appendix A. Supplementary data

Supplementary data to this article can be found online at https://doi.org/10.1016/j.jddst.2020.101562.

References

[1] S. Stegemann, F. Leveiller, D. Franchi, H. De Jong, H. Lindén, When poor solubility becomes an issue: from early stage to proof of concept, Eur. J. Pharmaceut. Sci. 31 (2007) 249–261.
[2] C.R. Gardner, C.T. Walsh, Ö. Almarsson, Drugs as materials: valuing physical form in drug discovery, Nat. Rev. Drug Discov. 3 (2004) 926–934.
[3] C.C. Sun, Cocrystallization for successful drug delivery, Expet Opin. Drug Deliv. 10 (2013) 201–213.
[4] G.R. Desiraju, Supramolecular synthons in crystal engineering—a new organic synthesis, Angew Chem. Int. Ed. Engl. 34 (1995) 2311–2327.
[5] N.K. Duggirala, M.L. Perry, Ö. Almarsson, M.J. Zaworotko, Pharmaceutical cocrystals: along the path to improved medicines, Chem. Commun. 52 (2016) 640–655.
[6] G.R. Desiraju, Crystal engineering: from molecule to crystal, J. Am. Chem. Soc. 135 (2013) 9952–9967.
[7] S. Cherukuvada, A. Nangia, Eutectics as improved pharmaceutical materials: design, properties and characterization, Chem. Commun. 50 (2014) 906–923.
[8] R.D. Patel, M.K. Raval, A.A. Bagathariya, N.R. Sheth, Functionality improvement of Nimesulide by eutectic formation with nicotinamide: exploration using temperature-composition phase diagram, Adv. Powder Technol. 30 (2019) 961–973.
[9] R. Chadha, M. Sharma, J. Haneef, Multicomponent solid forms of felodipine: preparation, characterisation, physicochemical and in-vivo studies, J. Pharm. Pharmacol. 69 (2017) 254–264.
[10] S.G. Khare, S.K. Jena, A.T. Sangamwar, S. Khullar, S.K. Mandal, Multicomponent pharmaceutical adducts of α-eprosartan: physicochemical properties and pharmacokinetic study, Cryst. Growth Des. 17 (2017) 1589–1599.
[11] I. Sathisaran, S.V. Dalvi, Crystal engineering of curcumin with salicylic acid and hydroxyquinol as coformers, Cryst. Growth Des. 17 (2017) 3974–3988.
[12] H. Jain, K.S. Khomane, A.K. Bansal, Implication of microstructure on the mechanical behaviour of an aspirin–paracetamol eutectic mixture, CrystEngComm 16 (2014) 8471–8478.
[13] A. Górniak, B. Karolewicz, E. Żurawska-Płaksej, J. Pluta, Thermal, spectroscopic, and dissolution studies of the simvastatin–acetylsalicylic acid mixtures, J. Therm. Anal. Calorim. 111 (2013) 2125–2132.
[14] R. Thipparaboina, D. Thumuri, R. Chavan, V.G. Naidu, N.R. Shastri, Fast dissolving drug-drug eutectics with improved compressibility and synergistic effects, Eur. J. Pharmaceut. Sci. 104 (2017) 82–89.
[15] J. Haneef, R. Chadha, Drug-drug multicomponent solid forms: cocrystal, coamorphous and eutectic of three poorly soluble antihypertensive drugs using mechanochemical approach, AAPS PharmSciTech 18 (2017) 2279–2290.
[16] T. Tamura, T. Yokoyama, K. Ohmori, Effects of diacerein on indomethacin-induced gastric ulceration, Pharmacology 63 (2001) 228–233.
[17] P. Nicolas, M. Tod, C. Padoin, O. Petitjean, Clinical pharmacokinetics of diacerein, Clin. Pharmacokinet. 35 (1998) 347–359.
[18] I. Elsayed, A.A. Abdelbary, A.H. Elshafeey, Nanosizing of a poorly soluble drug: technique optimization, factorial analysis, and pharmacokinetic study in healthy human volunteers, Int. J. Nanomed. 9 (2014) 2943–2953.
[19] D.K. Batt, K.C. Garala, Preparation and evaluation of inclusion complexes of diacerein with β-cyclodextrin and hydroxypropyl β-cyclodextrin, J. Inclusion Phenom. Macrocycl. Chem. 77 (2013) 471–481.
[20] H.M. El-Laithy, E.B. Basalious, B.M. El-Hoseiny, M.M. Adel, Novel self-nanoemulsifying self-nanosuspension (SNESNS) for enhancing oral bioavailability of diacerein: simultaneous portal blood absorption and lymphatic delivery, Int. J. Pharm. 490 (2015) 146–154.
[21] A.K. Aggarwal, S. Singh, Physicochemical characterization and dissolution study of solid dispersions of diacerein with polyethylene glycol 6000, Drug Dev. Ind. Pharm. 37 (2011) 1181–1191.
[22] A. Jain, S.K. Singh, Y. Singh, S. Singh, Development of lipid nanoparticles of diacerein, an antiosteoarthritic drug for enhancement in bioavailability and reduction in its side effects, J. Biomed. Nanotechnol. 9 (2013) 891–900.
[23] R. Malik, T. Garg, A.K. Goyal, G. Rath, Diacerein-Loaded novel gastroretentive nanofiber system using PLLA: development and in vitro characterization, Artif. Cells Nanomed. Biotechnol. 44 (2016) 928–936.
[24] S. Cherukuvada, A. Nangia, Fast dissolving eutectic compositions of two anti-tubercular drugs, CrystEngComm 14 (2012) 2579–2588.
[25] R. Kaur, R. Gautam, S. Cherukuvada, T.N. Guru Row, Do carboximide–carboxylic acid combinations form co-crystals? The role of hydroxyl substitution on the formation of co-crystals and eutectics, IUCr J. 2 (2015) 341–351.
[26] M. Maciejewski, T.J. Brunner, S.F. Loher, W.J. Stark, A. Baiker, Phase transitions in amorphous calcium phosphates with different Ca/P ratios, Thermochim. Acta 468 (2008) 75–80.
[27] L. Campanella, V. Micieli, M. Tomassetti, S. Vecchio, Solid–liquid phase diagrams of binary mixtures, J. Therm. Anal. Calorim. 99 (2010) 887–892.
[28] P.J. Denny, Compaction equations: a comparison of the Heckel and Kawakita equations, Powder Technol. 127 (2002) 162–172.
[29] J. Nordström, I. Klevan, G. Alderborn, A particle rearrangement index based on the Kawakita powder compression equation, J. Pharmaceut. Sci. 98 (2009) 1053–1063.
[30] S. Patel, A.M. Kaushal, A.K. Bansal, Compaction behavior of roller compacted ibuprofen, Eur. J. Pharm. Biopharm. 69 (2008) 743–749.
[31] B.S. Barot, P.B. Parejiya, T.M. Patel, R.K. Parikh, M.C. Gohel, Compactibility improvement of metformin hydrochloride by crystallization technique, Adv. Powder Technol. 23 (2012) 814–823.
[32] J.T. Fell, J.M. Newton, Determination of tablet strength by the diametral-compression test, J. Pharmaceut. Sci. 59 (1970) 688–691.
[33] N.A. Armstrong, R.F. Haines-Nutt, Elastic recovery and surface area changes in compacted powder systems, Powder Technol. 9 (1974) 287–290.
[34] Anonymous, Indian Pharmacopoeia vol. III, Government of India Ministry of Health & Family Welfare, The Indian Pharmacopoeia Commission, Ghaziabad, 2010, pp. 1191–1193.
[35] K.A. Khan, The concept of dissolution efficiency, J. Pharm. Pharmacol. 27 (1975) 48–49.
[36] P. Costa, J.M.S. Lobo, Modeling and comparison of dissolution profiles, Eur. J. Pharmaceut. Sci. 13 (2001) 123–133.
[37] K.D. Prasad, S. Cherukuvada, L.D. Stephen, T.N. G Row, Effect of inductive effect on the formation of cocrystals and eutectics, CrystEngComm 16 (2014) 9930–9938.
[38] S. Cherukuvada, T.N.G. Row, Comprehending the formation of eutectics and cocrystals in terms of design and their structural interrelationships, Cryst. Growth Des. 14 (2014) 4187–4198.
[39] E. Lu, N. Rodríguez-Hornedo, R. Suryanarayanan, A rapid thermal method for cocrystal screening, CrystEngComm 10 (2008) 665–668.
[40] T. Friscic, W. Jones, Recent advances in understanding the mechanism of cocrystal formation via grinding, Cryst. Growth Des. 9 (2009) 1621–1637.
[41] D.A. Haynes, W. Jones, W.S. Motherwell, Cocrystallisation of succinic and fumaric acids with lutidines: a systematic study, CrystEngComm 8 (2006) 830–840.
[42] E.V. Agafonova, Y.V. Moshchenskiy, M.L. Tkachenko, DSC study and calculation of metronidazole and clarithromycin thermodynamic melting parameters for individual substances and for eutectic mixture, Thermochim. Acta 580 (2014) 1–6.
[43] P.P. Shah, R.C. Mashru, Development and evaluation of artemether taste masked rapid disintegrating tablets with improved dissolution using solid dispersion technique, AAPS PharmSciTech 9 (2008) 494–500.
[44] T. Khan, R. Ranjan, Y. Dogra, S.M. Pandya, H. Shafi, S.K. Singh, P.N. Yadav, A. Misra, Intranasal eutectic powder of zolmitriptan with enhanced bioavailability in the rat brain, Mol. Pharm. 13 (2016) 3234–3240.
[45] M.K. Raval, K.R. Sorathiya, N.P. Chauhan, J.M. Patel, R.K. Parikh, N.R. Sheth, Influence of polymers/excipients on development of agglomerated crystals of secnidazole by crystallo-co-agglomeration technique to improve processability, Drug Dev. Ind. Pharm. 39 (2013) 437–446.
[46] A.B. Joshi, S. Patel, A.M. Kaushal, A.K. Bansal, Compaction studies of alternate solid forms of celecoxib, Adv. Powder Technol. 21 (2010) 452–460.
[47] G. Abdelbary, C. Eouani, P. Prinderre, J. Joachim, J.P. Reynier, P.H. Piccerelle, Determination of the in vitro disintegration profile of rapidly disintegrating tablets and correlation with oral disintegration, Int. J. Pharm. 292 (2005) 29–41.
[48] D. Gao, J.S. Wu, W.S. Lu, S. Chen, P.C. Kuo, C.M. Chen, ANCHEN LABORATORIES inc, 2010. Pharmaceutical compositions containing diacerein. U.S. Patent Application 12/607,251.
[49] N.J. Babu, A. Nangia, Solubility advantage of amorphous drugs and pharmaceutical cocrystals, Cryst. Growth Des. 11 (2011) 2662–2679.
[50] N.R. Goud, K. Suresh, P. Sanphui, A. Nangia, Fast dissolving eutectic compositions of curcumin, J. Pharmaceut. Sci. 439 (2012) 63–72.
[51] D.J. Good, N. Rodríguez-Hornedo, Cocrystal eutectic constants and prediction of solubility behavior, Cryst. Growth Des. 10 (2010) 1028–1032.
[52] A.H. Goldberg, M. Gibaldi, J.L. Kanig, Increasing dissolution rates and gastrointestinal absorption of drugs via solid solutions and eutectic mixtures III: experimental evaluation of griseofulvin-succinic acid solid solution, J. Pharmaceut. Sci. 55 (1966) 487–492.